

Neuronal activity modifies the chromatin accessibility landscape in the adult brain

Yijing Su^{1,2}, Jaehoon Shin^{1,2}, Chun Zhong^{1,2}, Sabrina Wang¹, Prith Roychowdhury¹, Jongseuk Lim¹, David Kim¹, Guo-li Ming¹⁻⁴ & Hongjun Song¹⁻³

Neuronal activity-induced gene expression modulates the function and plasticity of the nervous system. It is unknown whether and to what extent neuronal activity may trigger changes in chromatin accessibility, a major mode of epigenetic regulation of gene expression. Here we compared chromatin accessibility landscapes of adult mouse dentate granule neurons *in vivo* before and after synchronous neuronal activation using an assay for transposase-accessible chromatin using sequencing (ATAC-seq). We found genome-wide changes 1 h after activation, with enrichment of gained-open sites at active enhancer regions and at binding sites for AP1-complex components, including c-Fos. Some changes remained stable for at least 24 h. Functional analysis further implicates a critical role of c-Fos in initiating, but not maintaining, neuronal activity-induced chromatin opening. Our results reveal dynamic changes of chromatin accessibility in adult mammalian brains and suggest an epigenetic mechanism by which transient neuronal activation leads to dynamic changes in gene expression via modifying chromatin accessibility.

How transient activation of mature neuronal circuits leads to changes in gene expression and properties in neurons over the short- and long-term is a fundamental question in neurobiology and has significant implications for understanding neuronal plasticity, learning and memory, and brain disorders¹. Epigenetic mechanisms play a crucial role in regulating neuronal gene expression, and neuronal activity is known to alter epigenetic landmarks, such as DNA methylation and histone modifications²⁻¹¹. These epigenetic changes not only regulate which genes become activated or suppressed but also modify the dynamics of gene expression¹².

Regulation of chromatin opening is an important regulatory mechanism for the precise control of gene expression patterns. Global changes in chromatin accessibility occur during cell differentiation when cells with the same genome establish their identities through distinct gene expression patterns. Previous genome-wide studies of different tissues and cell types, including those in the nervous system, have revealed tissue- and cell-type-specific landscapes of chromatin accessibility¹³⁻¹⁶. Whether large-scale changes in chromatin accessibility occur after cell differentiation and maturation *in vivo* is unclear. Specifically, in the nervous system, whether and to what extent neuronal activity may reshape the accessible chromatin landscape in neurons and induce transient and sustained biological outcomes are largely unknown. Here we examined the impact of acute neuronal activation on chromatin accessibility and gene expression in dentate granule neurons over time in the adult mouse brain *in vivo*.

RESULTS

Widespread chromatin accessibility changes induced by neuronal activation

To investigate whether neuronal activation induces changes in chromatin accessibility, we employed an assay for transposase-accessible chromatin using sequencing (ATAC-seq) for sensitive and quantitative measurement of chromatin accessibility across the genome¹⁷ (Online Methods). We performed ATAC-seq of biological replicates ($n = 3$ or 4 for each condition) of microdissected dentate gyri before (E0 thereafter) and 1 h (E1 thereafter) after synchronous neuronal activation via electroconvulsive stimulation¹⁸⁻²⁰, a procedure currently used to treat patients with drug-resistant depression²¹. Our previous studies have shown that this *in vivo* preparation is highly enriched for dentate granule neurons (over 90%) and such treatment switches most neurons from an inactive state that reflects the presumed sparse coding in the dentate gyrus²² to an active state¹⁸⁻²⁰. We identified 89,946 and 114,959 open chromatin regions at E0 and E1, respectively ($P < 1 \times 10^{-5}$; **Supplementary Table 1**). We compared our data set to previously published chromatin-accessibility profiles of different tissues and cell types (**Supplementary Table 2**). The signature of open chromatin regions at the basal state (E0) is closer to those of different neuronal subtypes than to those of astrocytes or other non-neural tissues (**Supplementary Fig. 1**). We identified 16,882 open chromatin regions that occurred in dentate gyrus neurons but not in other cell types or tissues examined (**Supplementary Table 3**). Consistent with previous findings^{13,23,24}, open chromatin sites exhibited a broad

¹Institute for Cell Engineering, Johns Hopkins University School of Medicine, Baltimore, Maryland, USA. ²Department of Neurology, Johns Hopkins University School of Medicine, Baltimore, Maryland, USA. ³The Solomon H. Snyder Department of Neuroscience, Johns Hopkins University School of Medicine, Baltimore, Maryland, USA. ⁴Department of Psychiatry and Behavioral Sciences, Johns Hopkins University School of Medicine, Baltimore, Maryland, USA. Correspondence should be addressed to H.S. (shongju1@jhmi.edu).

Received 26 May 2016; accepted 31 December 2016; published online 6 February 2017; doi:10.1038/nn.4494

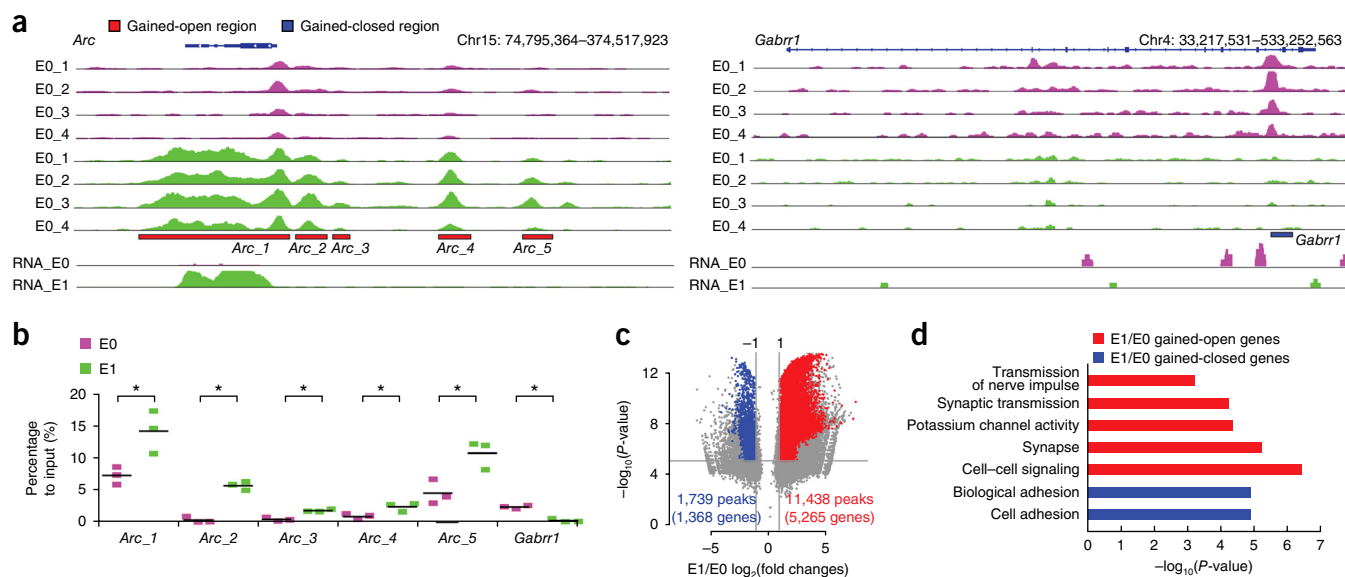


Figure 1 Modification of the chromatin accessibility landscape in the adult mouse dentate gyrus by transient neuronal activation. **(a)** UCSC genome browser (<https://genome.ucsc.edu/>) visualization of gained-open and gained-closed chromatin profiling coverage at the *Arc* and *Gabrr1* loci before (E0; magenta) and 1 h after synchronous neuronal activation (E1; green). Data from each individual sample are shown. Significant gained-open regions (red bars) and a gained-closed region (blue bar) are indicated ($P < 1 \times 10^{-5}$; fold changes > 2). **(b)** Summary of FAIRE-qPCR results for gained-open and gained-closed regions at the *Arc* and *Gabrr1* loci. Data from three individual samples for each condition are shown. Each line indicates the mean value. ($*P < 0.05$; permutation test). **(c)** Comparison of open chromatin profiles of the dentate gyrus of adult mice between E1 and E0. Differential regions are shown in a volcano plot. Gained-open sites are shown in red and gained-closed sites are shown in blue ($P < 1 \times 10^{-5}$; fold changes > 2 ; *t*-test; $n = 4$ mice in each group). **(d)** Gene ontology (GO) analysis of genes associated with gained-open (red) and gained-closed (blue) regions at E1 compared with E0.

genomic distribution, with the majority of peaks mapped to intergenic regions, introns and promoters of annotated genes (Supplementary Fig. 2a), and showed a positive correlation with the expression levels of associated genes (Supplementary Fig. 2b).

To determine how chromatin accessibility changes upon neuronal stimulation, we assessed quantitative differences in ATAC-seq signal intensities between E0 and E1. We observed marked chromatin accessibility changes at many regions in multiple independent samples, such as ‘gained-open’ at the *Arc* locus, which was correlated with induced gene expression, and ‘gained-closed’ at the *Gabrr1* locus, which was correlated with diminished gene expression (Fig. 1a). ATAC-seq is based on the activity of Tn5 (ref. 17). To validate chromatin accessibility changes at the *Arc* and *Gabrr1* loci using an independent approach, we performed formaldehyde-assisted isolation of regulatory elements (FAIRE)-quantitative (q) PCR (Fig. 1b). Overall, ATAC-seq analysis identified 11,438 gained-open and 1,739 gained-closed regions at E1 compared to E0 ($P < 1 \times 10^{-5}$; fold changes > 2 ; Fig. 1c and Supplementary Table 4). Gene ontology analysis of 5,265 genes associated with gained-open regions revealed enrichment of pathways related to cell–cell signaling, synapses and synaptic transmission (Fig. 1d). Together, these results indicate that transient neuronal activation modifies the chromatin accessibility landscape in neurons *in vivo*, largely through increased accessibility.

Genomic features and chromatin states of regions with chromatin accessibility changes

To characterize the genome-wide distribution of activity-induced chromatin accessibility changes, we used the HOMER software²⁵ for annotation of those gained-open and gained-closed regions. The majority of changes resided outside of promoter regions of annotated genes (Fig. 2a), consistent with the ability of ATAC-seq to identify distal regulatory elements in the genome^{17,26}. To determine the chromatin

state of regions with activity-induced accessibility changes, we compared our differential chromatin-accessibility data set with published profiles of histone modifications from adult mouse hippocampus tissue²⁷ and chromatin immunoprecipitation-sequencing (ChIP-seq) dataset for CCCTC-binding factor (CTCF) from the adult mouse cortex²⁸ (Supplementary Table 2). We observed overlap between gained-open regions and previously functionally identified enhancer regions^{29–31} at the *Arc* and *Fos* (hereinafter referred to as *c-Fos*) loci (Supplementary Fig. 3a). Across the genome, active enhancer histone marks^{32,33}, such as H3K4me1 and H3K27ac, were more enriched at gained-open and gained-closed regions than transcription repressive markers^{34,35}, such as H3K27me3 and H3K9me3 (Fig. 2b and Supplementary Fig. 3b). To gain more detailed insight into the chromatin state of regions with accessibility changes, we used ChromHMM software³⁶ to establish a chromatin state model defined by recurrent combinations of histone modifications using the ChIP-seq data set from the adult mouse hippocampus²⁷ and CTCF ChIP-seq data set from the adult mouse cortex²⁸. Gained-open and gained-closed regions were found to be significantly enriched at active enhancers, as comarked by H3K4me1 and H3K27Ac (Fig. 2c and Supplementary Fig. 3c). Chromatin-accessibility changes also occurred near transcriptional start sites (TSS), as comarked by H3K4me3 and H3K27ac (Fig. 2c and Supplementary Fig. 3c). We next asked whether chromatin accessibility was specifically correlated with histone modifications that are also sensitive to neuronal activity. We employed the published histone modification ChIP-seq data set³² from cultured neurons before and after KCl treatment, including H3K4me1, H3K4me3, H3K27ac and H3K27me3, and found that neither gained-open nor gained-closed regions were enriched in changes for those four histone marks (Supplementary Fig. 4).

To assess the potential biological significance of activity-induced chromatin accessibility changes, we first identified 4,455 and 558

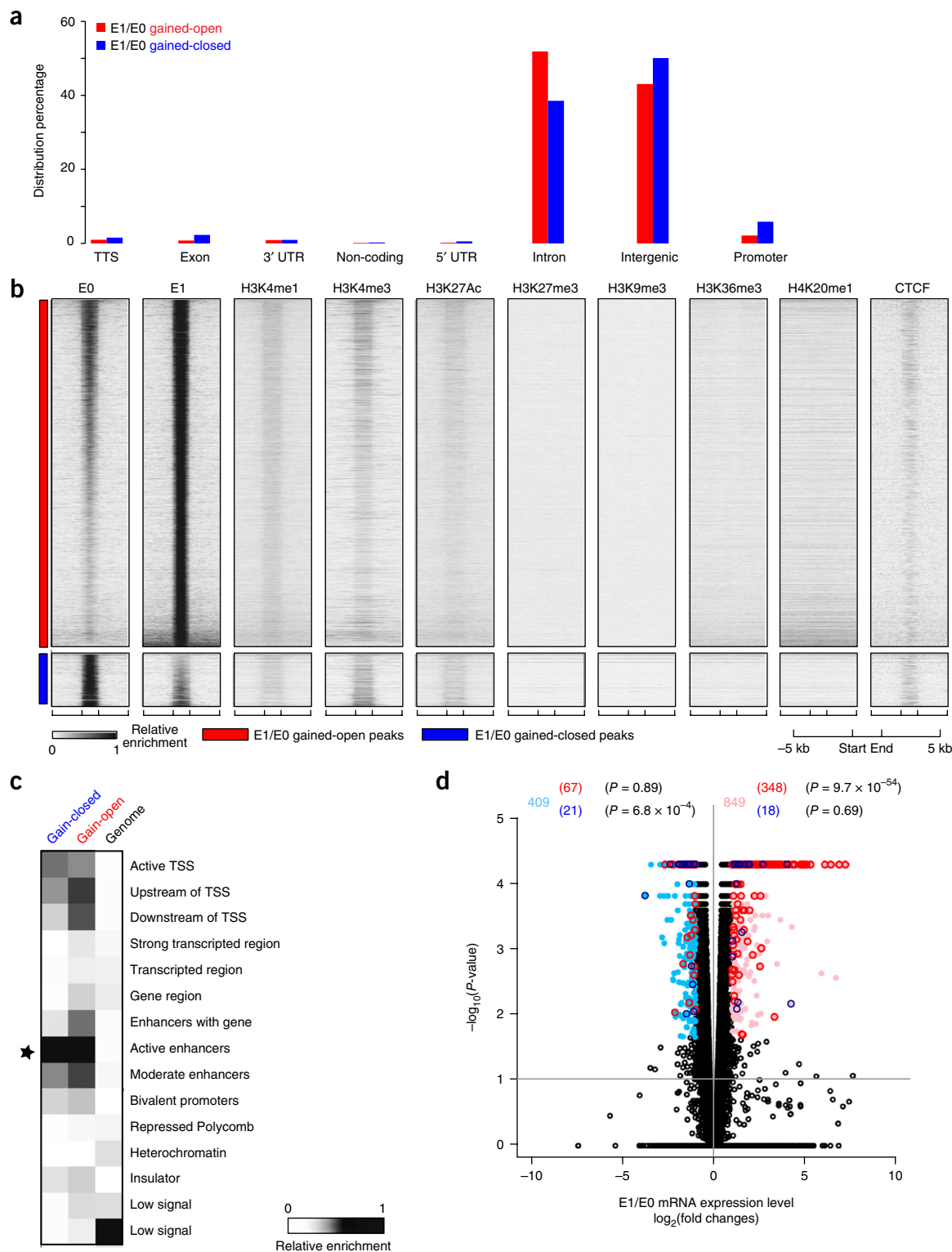


Figure 2 Characterization of gained-open and gained-closed regions at E1 compared to E0. **(a)** Genomic features of gained-open ($n = 11,438$) and gained-closed regions ($n = 1,739$) at E1. **(b)** Genomic regions with neuronal activation-induced changes in chromatin accessibility are enriched with H3K4me1 and H3K27Ac active histone marks but not with histone modifications for repressive (H3K27me3) markers. Regions between start and end define boundaries of differential sites. ChIP-seq mapped reads of various histone modifications²⁷ and CTCF²⁸ (see **Supplementary Table 2** for data sources) were plotted in heat-map views. **(c)** Characterization of histone modification states of gained-open and gained-closed regions using ChromHMM. The star indicates active enhancers, the sites of the greatest enrichment of gained-open and gained-closed regions. **(d)** Expression levels of genes associated with gained-open and gained-closed regions between E0 and E1. Color coding indicates significantly upregulated (pink) and downregulated (light blue) genes between E1 and E0, as well as those overlapped with genes associated with gained-open peaks (red) or with genes associated with gained-closed peaks (blue) ($P < 0.05$; fold changes > 2 ; Fisher's exact test).

genes that contained only gained-open or gained-closed regions at E1 compared to E0, respectively. We next performed RNA-seq analysis and identified 849 upregulated genes and 409 downregulated genes at E1 compared to E0 ($P < 0.05$; fold changes > 2 ; Fig. 2d and Supplementary Table 5). Comparison of these two data sets showed significant overlap of genes associated with gained-open peaks with upregulated genes ($P = 9.7 \times 10^{-54}$) but not downregulated genes ($P = 0.89$; Fig. 2d). In addition, we found a significant overlap of genes associated with gained-closed peaks with downregulated genes ($P = 6.8 \times 10^{-4}$) but not with upregulated genes ($P = 0.69$; Fig. 2d). Together, these results indicate that neuronal activation led to chromatin accessibility changes enriched at active enhancer regions, which in turn govern gene expression. Further, we observed that genes associated with chromatin opening were more likely to be upregulated, whereas genes associated with chromatin closing were more likely to be downregulated.

Role of c-Fos in activity-induced chromatin opening

Next we performed *de novo* motif analyses using MEME-ChIP (ref. 37) and HOMER software²⁵ to identify transcription factors associated with regions with chromatin accessibility changes. Unbiased motif discovery analyses of gained-open regions identified a DNA logo with striking resemblance to the binding motif of the AP-1 complex, especially the c-Fos, fosB and c-Jun subunits, which are encoded by classic neuronal activity-induced immediate-early genes³⁸ ($P = 1.7 \times 10^{-1,120}$; Fig. 3a and Supplementary Fig. 5a,c). About 78.9% of 11,438 gained-open regions at E1 contained the logo (Fig. 3b) and there was a significant overlap between gained-open regions and c-Fos ChIP-seq peaks³² ($P < 1 \times 10^{-6}$; Fig. 3c and Supplementary Table 6). Further genome-wide analysis revealed increased chromatin accessibility at binding sites for c-Fos, fosB and jun-B, but not CREB, indicating specificity (Fig. 3d). In addition, there was increased ChIP signal for c-Fos, fosB and jun-B, but not CREB, at activity-induced gained-open, but not gained-closed, regions (Fig. 3e). In contrast, the DNA logo identified using MEME-ChIP³⁷ and HOMER²⁵ for gained-closed regions did not match any known transcription factor binding motifs ($P = 4.5 \times 10^{-51}$; Supplementary Fig. 5b,c).

Given that AP-1 subunits are encoded by well-known activity-induced immediate-early genes³⁹, the coincidence of AP-1 binding and neuronal activity-induced chromatin opening raises the possibility that AP-1 subunits play a functional role in chromatin opening. To test this hypothesis, we focused on c-Fos and first asked whether it is required for activity-induced chromatin opening at regions with c-Fos binding sites. We confirmed the induction of *c-Fos* expression in our experimental model at both mRNA and protein levels (Supplementary Fig. 6a,b). We used a previously established adeno-associated virus (AAV2/9) to co-express EYFP and shRNAs in the adult mouse dentate gyrus^{20,40} (Supplementary Fig. 6c). Expression of shRNA against mouse *c-Fos* (shRNA-cFos), but not control shRNA (shRNA-Ctrl), effectively reduced neuronal activity-induced endogenous *c-Fos* expression as examined by qPCR and RNA-seq (Supplementary Figs. 6d and 7a). We performed ATAC-seq of dentate gyri expressing shRNA-Ctrl or shRNA-cFos at E0 and E1 (Fig. 4a,b and Supplementary Fig. 7b). Knockdown of *c-Fos* attenuated neuronal activity induced-chromatin opening at c-Fos binding sites (Fig. 4a,c, Supplementary Fig. 7c and Supplementary Table 7). RNA-seq analysis further showed that activity-induced upregulation of genes associated with these sites was significantly attenuated (Fig. 4d and Supplementary Table 5). Notably, 72.1% of upregulated genes ($P < 0.05$; fold changes > 2) in control neurons at E1 lost responsiveness in *c-Fos*-knockdown neurons (Supplementary Fig. 7d).

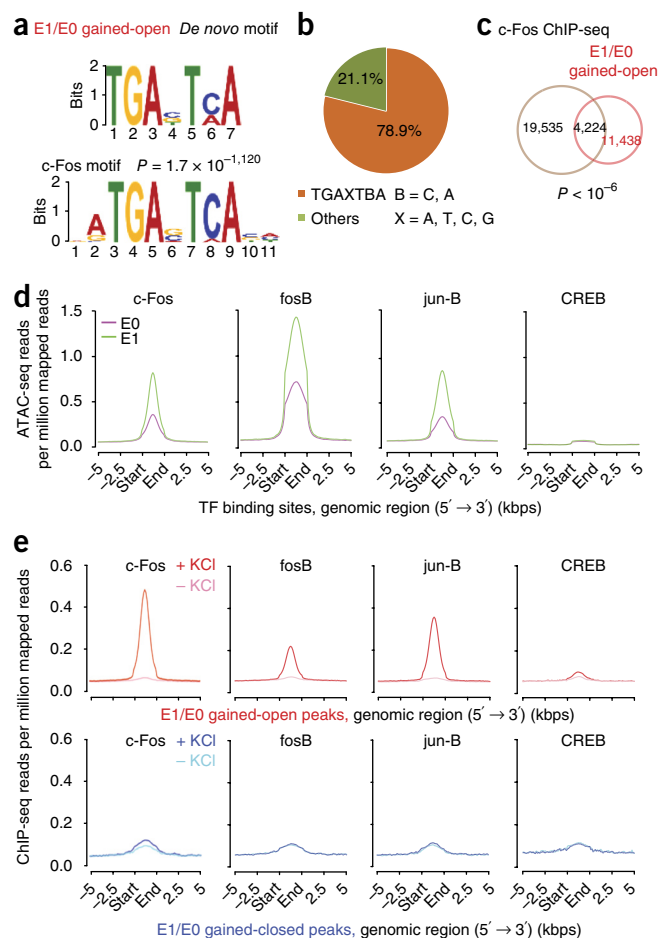


Figure 3 Enrichment of c-Fos binding sites at neuronal activity-induced chromatin opening regions. (a) Common motifs within chromatin gained-open regions at E1 (top) predicted using MEME-ChIP (ref. 43). (b) Pie chart of gained-open peaks with the specific DNA logo. (c) Venn diagram of c-Fos ChIP binding sites and chromatin gained-open regions at E1. (d) Aggregate plots of ATAC-seq signals centered at c-Fos, fosB, jun-B and CREB binding sites at E0 and E1. (e) Aggregate plots of c-Fos, fosB, jun-B and CREB signals before and after KCl stimulation centered at gained-open (top panel) and gained-closed (bottom panel) sites at E1. The ChIP-seq data used for plots are from a previously published data set³².

Together, these results suggest that c-Fos expression is required for neuronal activity-induced chromatin opening at c-Fos binding sites and subsequent upregulation of associated genes.

We next asked whether exogenous c-Fos expression in dentate granule neurons *in vivo* is sufficient to induce chromatin opening at c-Fos binding sites. We used AAV to overexpress c-Fos and/or EYFP (Supplementary Fig. 6c,e) and performed ATAC-seq on dentate gyri in the absence of neuronal stimulation (Fig. 4a,e and Supplementary Table 7). Compared to EYFP expression alone, c-Fos overexpression partially mimicked neuronal activity-induced chromatin opening at regions with c-Fos binding sites (Fig. 4a,f). Among 647 chromatin gained-open regions induced by c-Fos overexpression, 56% overlapped with those induced by neuronal activity at E1 (Supplementary Fig. 7e). RNA-seq analysis further showed that genes associated with c-Fos-induced chromatin opening exhibited upregulated expression similar to that induced by neuronal activation (Fig. 4g). Together, these results support the model asserting that neuronal activity-induced expression of the immediate-early gene *c-Fos*

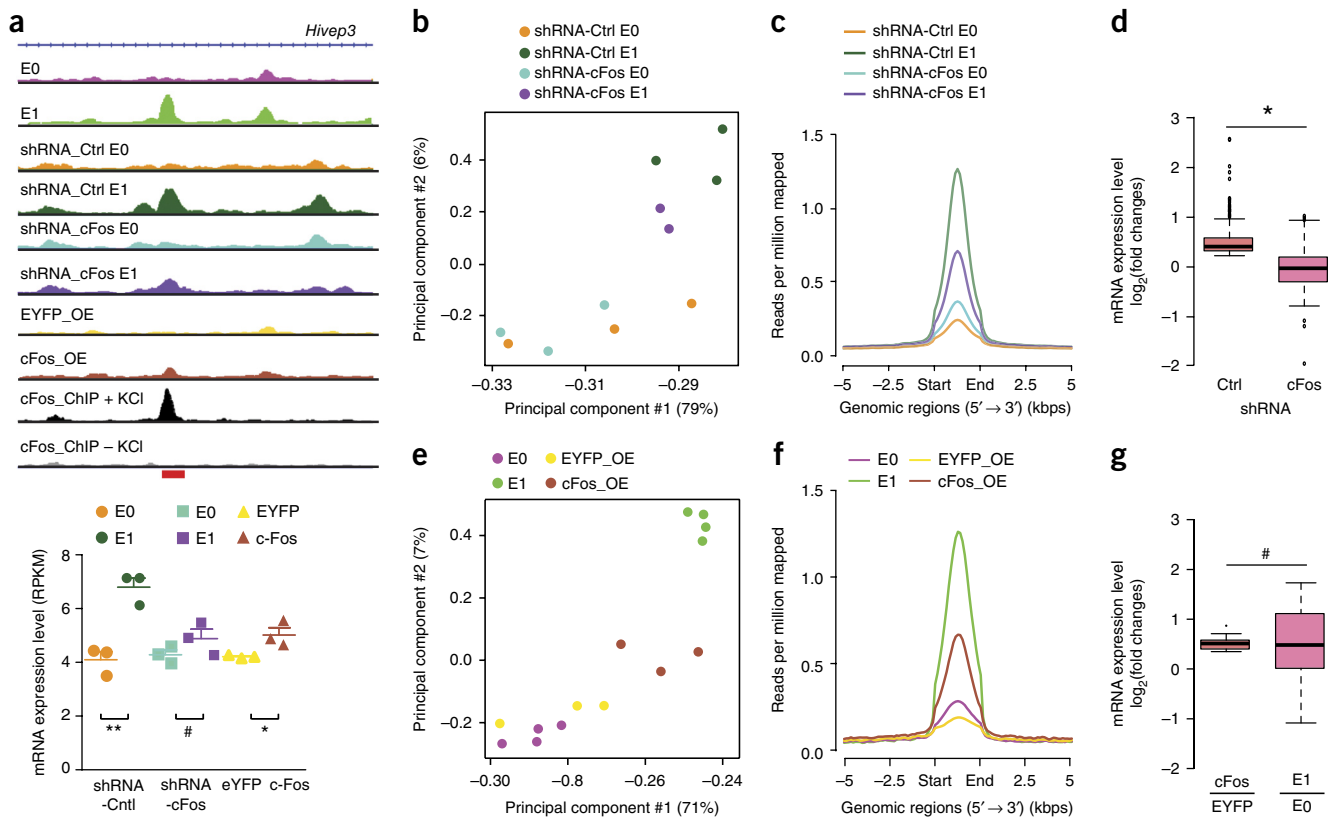


Figure 4 Critical role of c-Fos in neuronal activity-induced chromatin opening of regions with c-Fos binding sites. **(a)** UCSC genome browser visualization of ATAC-seq profiles at the *Hivexp3* locus under different conditions (chr4: 119,598,001–119,612,056; top panels). Data from merged biological replicates ($n = 2$ or 3 mice in each group) are shown. Red bar indicates the region where *c-Fos* knockdown blocked activity-induced chromatin opening. Also shown is a plot of expression levels of *Hivexp3* under different conditions (bottom panel; $n = 3$ mice in each groups; $*P < 0.05$; $**P < 0.01$; $\#P > 0.1$; permutation test). Lines represent mean \pm s.e.m. **(b)** Principal component analysis of ATAC-seq of neurons expressing shRNA-Ctrl and shRNA-cFos at E0 and E1. **(c)** Aggregate plot of ATAC-seq signals centered on neuronal activity-induced gained-open regions with c-Fos binding sites for neurons expressing shRNA-Ctrl and shRNA-cFos at E0 and E1. **(d)** Box-plot of mean expression levels of upregulated genes in neurons expressing shRNA-Ctrl and shRNA-cFos in response to neuronal activation ($*P < 0.01$; Wilcoxon rank-sum test; $P < 2.2 \times 10^{-16}$). Center line, median value; box limits, 25th and 75th percentile values; whiskers, maximum and minimum data points excluding outliers; outliers, data points higher or lower than $1.5 \times$ the quartile (25th and 75th percentile) values. **(e)** Principal component analysis of ATAC-seq of neurons overexpressing EYFP or c-Fos in the absence of neuronal stimulation. **(f)** Aggregate plot of ATAC-seq analysis of neurons at E0 and E1 and neurons overexpressing c-Fos (c-Fos-OE) and/or EYFP (EYFP-OE) at E0, as in **(c)**. **(g)** Box-plot of mean expression levels of upregulated genes induced by c-Fos expression at E0 or neuronal activation at E1 without exogenous c-Fos expression; as in **(d)** ($\#P > 0.01$; Wilcoxon rank-sum test; $P = 0.81$).

mediates chromatin opening at its binding sites, resulting in upregulated expression of associated genes.

Temporal characteristics of activity-induced neuronal chromatin accessibility changes

To evaluate whether neuronal activity-induced chromatin accessibility changes are sustained over time following a single stimulation, we additionally performed ATAC-seq at 4 h (E4) and 24 h (E24) after synchronous neuronal activation (Supplementary Table 1). Comparison of data sets from different time points revealed many gained-open and gained-closed peaks at E4 and E24 compared to E0 (Fig. 5a,b; Supplementary Fig. 8a and Supplementary Table 4). Notably, 4,175 of 11,438 (36.5%) activity-induced gained-open peaks at E1 remained open at E4, and 597 (5%) remained open until E24 (Fig. 5b and Supplementary Table 3). Overall, there were 517 genes associated with sustained gained-open and 22 genes with sustained gained-closed peaks for 24 h (Fig. 5c and Supplementary Table 4). Gene ontology analysis of genes associated with sustained gained-open peaks over 24 h revealed enrichment of pathways related to axon guidance, cell signaling and cell adhesion (Fig. 5d).

As at E1, the majority of changes at E4 and E24 were distributed across the genome, mostly in introns and intergenic regions (Supplementary Fig. 8b,c).

We also characterized the chromatin state on those sustained gained-open peaks at E4 and E24 using ChromHMM (Fig. 6a). Gained-open peaks sustained for 4 h were enriched at active enhancers and a subset were located near TSS, whereas gained-open peaks sustained for 24 h were more enriched at sites upstream of TSS (Fig. 6b). Comparison of RNA-seq data from E1 and E4 to E0 identified 114 upregulated genes and 58 downregulated genes at both E1 and E4 ($P < 0.05$; fold changes > 2 ; Fig. 6c). There was a significant overlap of genes associated with gained-open peaks sustained for 4 h with upregulated genes ($P = 8.2 \times 10^{-27}$) but not with downregulated genes ($P = 0.68$; Fig. 6c). RNA-seq analysis at E24 revealed 15 genes upregulated at all three time points (E1, E4 and E24), three of which were associated with gained-open sites sustained for 24 h ($P = 3.8 \times 10^{-3}$).

The *de novo* motif discovery analysis of gained-open peaks sustained at E4 and E24 revealed DNA logos that resemble the binding motif of AP-1 ($P = 5.1 \times 10^{-479}$ for E4; $P = 5.4 \times 10^{-397}$ for E24; Fig. 7a). Approximately 44.8% and 60.6% of those gained-open peaks

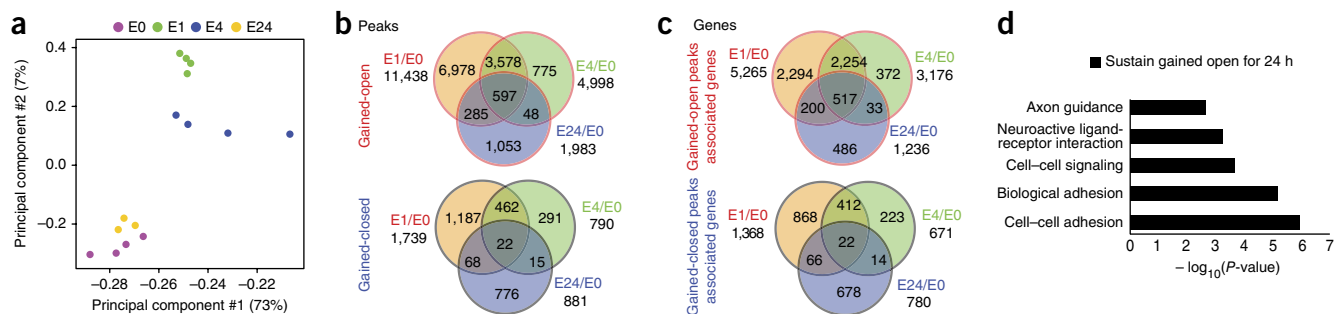


Figure 5 Characterization of neuronal activity-induced chromatin accessibility changes at different timepoints. **(a)** Principal component analysis of ATAC-seq data sets. Each dot represents data from one sample and is colored coded for before (E0) and 1 h (E1), 4 h (E4) or 24 h (E24) after synchronous neuronal activation. **(b,c)** Venn diagrams of **(b)** differential chromatin-accessible regions and **(c)** their associated genes. **(d)** GO analysis of genes with sustained gained-open chromatin accessibility for at least 24 h.

sustained for 4 h and 24 h overlap with c-Fos binding sites, respectively (Fig. 7b). One hallmark property of immediate-early genes is their transient expression³⁸. Synchronous neuronal activity led to transient c-Fos protein expression at 1 h, which became barely detectable at

4 h (Supplementary Fig. 6b). We selected multiple sustained gained-open regions associated with different genes for confirmation using c-Fos ChIP-qPCR analyses. Indeed, we could detect a significant association of c-Fos at these genomic loci at E1 but not at E0 or E4

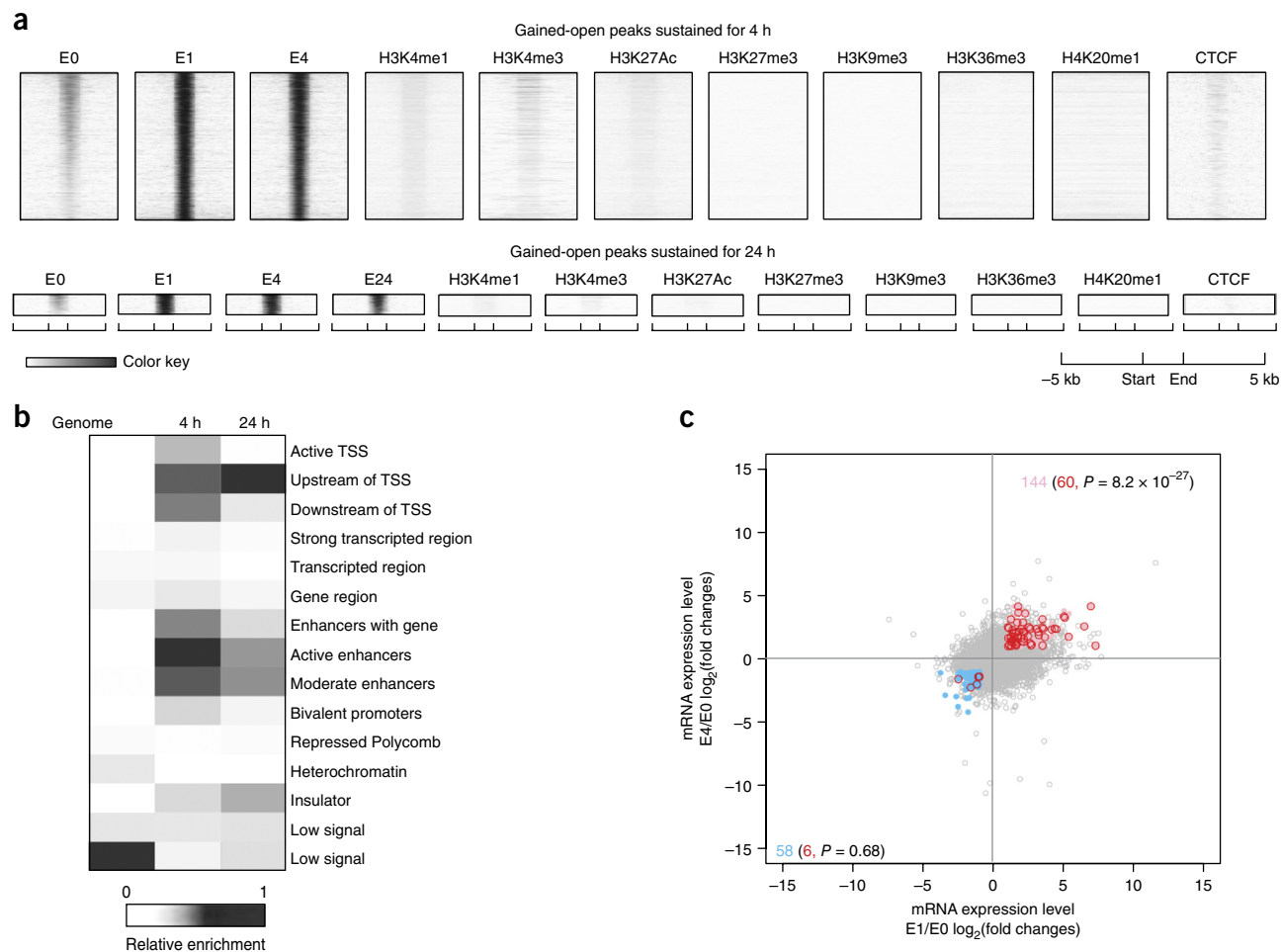


Figure 6 Characterization of chromatin-accessibility gained-open regions sustained for 4 h and 24 h. **(a)** Genomic regions with gained-opening sustained for 4 h and 24 h are enriched with H3K4me1 and H3K27Ac active histone marks but not with histone modifications for repressive (H3K27me3) markers. As in Figure 2b. **(b)** Characterization of histone-modification states of gained-open regions sustained for 4 h and 24 h using ChromHMM. As in Figure 2c. **(c)** Expression levels of genes associated with gained-open regions sustained for 4 h at E1 and E4. Significantly upregulated (pink) and downregulated (light blue) genes at E1 and E4 compared to E0; those overlapped with genes associated with gained-open peaks sustained for 4 h are coded in red ($P < 0.05$; fold changes > 2).

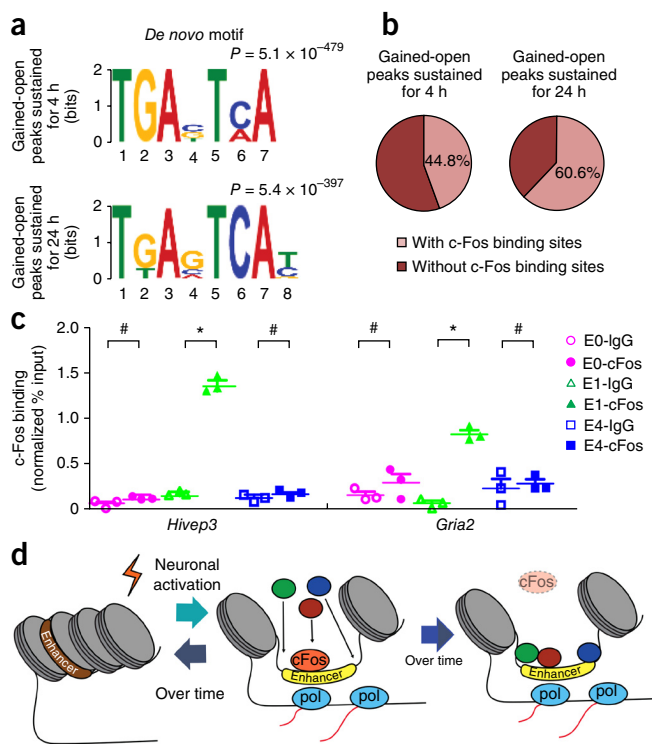


Figure 7 Gained-open sites can be maintained without c-Fos occupation. (a) Common motifs within chromatin gained-open regions sustained for 4 h (top panel) and 24 h (bottom panel) predicted using MEME-ChIP⁴³. (b) Pie chart of gained-open regions sustained for 4 h and 24 h with c-Fos binding sites. (c) ChIP of c-Fos and IgG followed by qPCR analysis of *Hiv1p3* and *Gria2* loci in the adult dentate gyrus at E0, E4 and E24 (normalized percentage input). Data from individual samples are shown (# $P > 0.05$; permutation test). Lines represent mean \pm s.e.m. (d) A working model for neuronal activity-induced changes in chromatin accessibility and dynamic changes in neuronal gene expression over time. * $P < 0.05$.

(Fig. 7c and Supplementary Fig. 9). Together, these results suggest a model asserting that c-Fos is required for the initiation, but not the maintenance, of neuronal activity-induced chromatin opening of regions with c-Fos binding sites over time (Fig. 7d).

DISCUSSION

It is now well established that activity-induced reshaping of transcriptomes plays a fundamental role in regulating neuronal properties, synaptic plasticity and cognitive function, as well as in various brain disorders^{2–8,41,42}. In addition to classic modes of epigenetic regulation via DNA and histone modifications, here we show that neuronal activity dynamically regulates the chromatin accessibility landscape in mature mammalian neurons *in vivo*. Genes associated with gained chromatin opening are enriched in pathways related to cell–cell signaling, synapses and synaptic transmission. Future studies will address how physiological stimuli, such as those encountered during explicit learning tasks, impact chromatin accessibility in individual neurons *in vivo*. The large ATAC-seq and RNA-seq data sets from dentate granule neurons *in vivo*, a relatively pure population of a single neuronal subtype in the adult mammalian brain¹⁹, at several time points after synchronous neuronal activation, can provide a useful resource for the neuroscience field and beyond.

Neuronal activity-induced gene expression is known to be very dynamic. The most well-known activity-induced genes are a set of immediate-early genes that includes *c-Fos* and *Jun* (refs. 38,39).

In the classic model, it is believed that these transcription factors are rapidly induced by neuronal activity and then removed to allow transient regulation of downstream gene expression via binding to their genomic binding sites. Our unbiased motif analysis revealed coincident AP-1 binding sites and neuronal activity-induced chromatin opening regions. Further gain- and loss-of-function analyses of the AP-1 subunit c-Fos suggested an important role of c-Fos in the induction, but not maintenance, of neuronal activity-induced chromatin opening. We propose a model indicating that, in addition to direct and acute regulation of their target genes, transcription factors encoded by immediate early genes, such as *c-Fos*, can play additional roles as epigenetic regulators to modify chromatin accessibility around a subset of their binding sites across the genome.

Our time-course analysis of the neuronal chromatin accessibility landscape upon acute activation showed that around 36.5% of the gained-open regions at 1 h remained open for at least 4 h and 5.1% remained for at least 24 h, whereas 27.8% of the gained-closed regions at 1 h remained closed up to 4 h later and 1.3% remained closed up to 24 h (Fig. 5). A previous study of the same preparation showed that 31% of activity-induced changes in CpG methylation at 4 h are maintained at 24 h (ref. 19). Therefore, compared to CpG DNA modification, activity-induced chromatin accessibility changes are relatively transient and reversible in neurons *in vivo*. Comparison of our chromatin accessibility data sets with previously published ChIP-seq data sets for various histone modifications revealed the enrichment of neuronal activity-induced chromatin accessibility changes on active enhancer regions. Furthermore, RNA-seq analysis showed a significant correlation between gained-opened or gain-closed regions and upregulation or downregulation, respectively, of associated genes. Given a large number of genes associated with gained-open and gained-closed regions at different timepoints after acute neuronal activation, our study therefore suggests a potential mechanism for how transient neuronal activation leads to dynamic changes in the expression of different sets of neuronal genes over time.

METHODS

Methods, including statements of data availability and any associated accession codes and references, are available in the online version of the paper.

Note: Any Supplementary Information and Source Data files are available in the online version of the paper.

ACKNOWLEDGMENTS

We thank the members of the Song and Ming laboratories for discussions, K. Christian for comments and Y. Cai and L. Liu for technical support. This work was supported by NIH (R37NS047344 and P01NS097206 to H.S., R35NS097370 and R01MH105128 to G.-I.M.), SFARI (Award 240011 to H.S.), The Dr. Miriam and Sheldon G. Adelson Medical Research Foundation (to G.-I.M.) and The Brain and Behavior Research Foundation (to Y.S.).

AUTHOR CONTRIBUTIONS

Y.S. and H.S. designed the project. C.Z. prepared the AAV and performed viral injections; Y.S., J.S., S.W., P.R., J.L. and D.K. contributed to data collection, analyses and interpretation. Y.S., J.S., G.-I.M. and H.S. wrote the manuscript.

COMPETING FINANCIAL INTERESTS

The authors declare no competing financial interests.

Reprints and permissions information is available online at <http://www.nature.com/reprints/index.html>.

1. Crick, F. Memory and molecular turnover. *Nature* **312**, 101 (1984).
2. Gräff, J., Kim, D., Dobbin, M.M. & Tsai, L.H. Epigenetic regulation of gene expression in physiological and pathological brain processes. *Physiol. Rev.* **91**, 603–649 (2011).

3. West, A.E. & Greenberg, M.E. Neuronal activity-regulated gene transcription in synapse development and cognitive function. *Cold Spring Harb. Perspect. Biol.* <http://dx.doi.org/10.1101/cshperspect.a005744> (2011).
4. Sweatt, J.D. The emerging field of neuroepigenetics. *Neuron* **80**, 624–632 (2013).
5. Descalzi, G. *et al.* Epigenetic mechanisms of chronic pain. *Trends Neurosci.* **38**, 237–246 (2015).
6. Lattal, K.M. & Wood, M.A. Epigenetics and persistent memory: implications for reconsolidation and silent extinction beyond the zero. *Nat. Neurosci.* **16**, 124–129 (2013).
7. Meaney, M.J. & Ferguson-Smith, A.C. Epigenetic regulation of the neural transcriptome: the meaning of the marks. *Nat. Neurosci.* **13**, 1313–1318 (2010).
8. Borrelli, E., Nestler, E.J., Allis, C.D. & Sassone-Corsi, P. Decoding the epigenetic language of neuronal plasticity. *Neuron* **60**, 961–974 (2008).
9. Guo, J.U., Su, Y., Zhong, C., Ming, G.L. & Song, H. Emerging roles of TET proteins and 5-hydroxymethylcytosines in active DNA demethylation and beyond. *Cell Cycle* **10**, 2662–2668 (2011).
10. Cholewa-Waclaw, J. *et al.* The role of epigenetic mechanisms in the regulation of gene expression in the nervous system. *J. Neurosci.* **36**, 11427–11434 (2016).
11. Weng, Y.L., An, R., Shin, J., Song, H. & Ming, G.L. DNA modifications and neurological disorders. *Neurotherapeutics* **10**, 556–567 (2013).
12. Jaenisch, R. & Bird, A. Epigenetic regulation of gene expression: how the genome integrates intrinsic and environmental signals. *Nat. Genet.* **33** (Suppl.), 245–254 (2003).
13. Vierstra, J. *et al.* Mouse regulatory DNA landscapes reveal global principles of cis-regulatory evolution. *Science* **346**, 1007–1012 (2014).
14. Schmid, R.S. *et al.* Core pathway mutations induce de-differentiation of murine astrocytes into glioblastoma stem cells that are sensitive to radiation but resistant to temozolomide. *Neuro-oncol.* **18**, 962–973 (2016).
15. Mo, A. *et al.* Epigenomic signatures of neuronal diversity in the mammalian brain. *Neuron* **86**, 1369–1384 (2015).
16. Shin, J., Ming, G.L. & Song, H. Decoding neural transcriptomes and epigenomes via high-throughput sequencing. *Nat. Neurosci.* **17**, 1463–1475 (2014).
17. Buenostro, J.D., Giresi, P.G., Zaba, L.C., Chang, H.Y. & Greenleaf, W.J. Transposition of native chromatin for fast and sensitive epigenomic profiling of open chromatin, DNA-binding proteins and nucleosome position. *Nat. Methods* **10**, 1213–1218 (2013).
18. Ma, D.K. *et al.* Neuronal activity-induced Gadd45b promotes epigenetic DNA demethylation and adult neurogenesis. *Science* **323**, 1074–1077 (2009).
19. Guo, J.U. *et al.* Neuronal activity modifies the DNA methylation landscape in the adult brain. *Nat. Neurosci.* **14**, 1345–1351 (2011).
20. Guo, J.U., Su, Y., Zhong, C., Ming, G.L. & Song, H. Hydroxylation of 5-methylcytosine by TET1 promotes active DNA demethylation in the adult brain. *Cell* **145**, 423–434 (2011).
21. Lisanby, S.H. Electroconvulsive therapy for depression. *N. Engl. J. Med.* **357**, 1939–1945 (2007).
22. Neunuebel, J.P. & Knierim, J.J. Spatial firing correlates of physiologically distinct cell types of the rat dentate gyrus. *J. Neurosci.* **32**, 3848–3858 (2012).
23. Thurman, R.E. *et al.* The accessible chromatin landscape of the human genome. *Nature* **489**, 75–82 (2012).
24. Frank, C.L. *et al.* Regulation of chromatin accessibility and Zic binding at enhancers in the developing cerebellum. *Nat. Neurosci.* **18**, 647–656 (2015).
25. Heinz, S. *et al.* Simple combinations of lineage-determining transcription factors prime cis-regulatory elements required for macrophage and B cell identities. *Mol. Cell* **38**, 576–589 (2010).
26. Davie, K. *et al.* Discovery of transcription factors and regulatory regions driving in vivo tumor development by ATAC-seq and FAIRE-seq open chromatin profiling. *PLoS Genet.* **11**, e1004994 (2015).
27. Gjonneska, E. *et al.* Conserved epigenomic signals in mice and humans reveal immune basis of Alzheimer's disease. *Nature* **518**, 365–369 (2015).
28. Shen, Y. *et al.* A map of the cis-regulatory sequences in the mouse genome. *Nature* **488**, 116–120 (2012).
29. Pintchovski, S.A., Peebles, C.L., Kim, H.J., Verdin, E. & Finkbeiner, S. The serum response factor and a putative novel transcription factor regulate expression of the immediate-early gene *Arcl/Arg3.1* in neurons. *J. Neurosci.* **29**, 1525–1537 (2009).
30. Kim, T.K. *et al.* Widespread transcription at neuronal activity-regulated enhancers. *Nature* **465**, 182–187 (2010).
31. Kawashima, T. *et al.* Synaptic activity-responsive element in the *Arcl/Arg3.1* promoter essential for synapse-to-nucleus signaling in activated neurons. *Proc. Natl. Acad. Sci. USA* **106**, 316–321 (2009).
32. Malik, A.N. *et al.* Genome-wide identification and characterization of functional neuronal activity-dependent enhancers. *Nat. Neurosci.* **17**, 1330–1339 (2014).
33. Shlyueva, D., Stampfel, G. & Stark, A. Transcriptional enhancers: from properties to genome-wide predictions. *Nat. Rev. Genet.* **15**, 272–286 (2014).
34. Young, M.D. *et al.* ChIP-seq analysis reveals distinct H3K27me3 profiles that correlate with transcriptional activity. *Nucleic Acids Res.* **39**, 7415–7427 (2011).
35. Barski, A. *et al.* High-resolution profiling of histone methylations in the human genome. *Cell* **129**, 823–837 (2007).
36. Ernst, J. & Kellis, M. Discovery and characterization of chromatin states for systematic annotation of the human genome. *Nat. Biotechnol.* **28**, 817–825 (2010).
37. Machanick, P. & Bailey, T.L. MEME-ChIP: motif analysis of large DNA datasets. *Bioinformatics* **27**, 1696–1697 (2011).
38. Curran, T. & Morgan, J.I. Fos: an immediate-early transcription factor in neurons. *J. Neurobiol.* **26**, 403–412 (1995).
39. Nedivi, E., Hevroni, D., Naot, D., Israeli, D. & Citri, Y. Numerous candidate plasticity-related genes revealed by differential cDNA cloning. *Nature* **363**, 718–722 (1993).
40. Jang, M.H. *et al.* Secreted frizzled-related protein 3 regulates activity-dependent adult hippocampal neurogenesis. *Cell Stem Cell* **12**, 215–223 (2013).
41. De Rubeis, S. *et al.* Synaptic, transcriptional and chromatin genes disrupted in autism. *Nature* **515**, 209–215 (2014).
42. Felling, R.J. & Song, H. Epigenetic mechanisms of neuroplasticity and the implications for stroke recovery. *Exp. Neurol.* **268**, 37–45 (2015).
43. Ma, W., Noble, W.S. & Bailey, T.L. Motif-based analysis of large nucleotide data sets using MEME-ChIP. *Nat. Protoc.* **9**, 1428–1450 (2014).

ONLINE METHODS

Animals. Adult male, 8–10-week-old mice on a C57BL/6 background were housed in a standard facility. All animal procedures used in this study were performed in accordance with protocols approved by the Institutional Animal Care and Use Committee of Johns Hopkins University School of Medicine. Synchronous neuronal activation of dentate granule neurons *in vivo* was achieved via electroconvulsive stimulation, which was administered with 1.0 s stimuli (total duration) consisting of 100-Hz, 16–18-mA, 0.3-ms pulses delivered using a Ugo Basile ECT unit (Ugo Basile, Collevalle, model 57800) as previously described^{18,19}. Control mice were similarly handled in parallel without the electrical current delivery. Previous studies using Western blots and immunostaining of the activated form of caspase (Caspase-3a) and phosphorylated ataxia telangiectasia mutated kinase (ATM) showed that such treatment does not cause any detectable damage¹⁸. For AAV-based genetic manipulation, the recombinant AAV vectors were serotyped with AAV2/9. High titers of engineered AAV2/9 virus were stereotaxically injected into adult mouse dentate gyrus as previously described^{44,45}. One week after viral injection, animals were subject to sham or electroconvulsive stimulation. Dentate gyrus region was rapidly fresh dissected from adult mouse hippocampus under a dissection microscope. Previous studies have shown that such preparations are highly enriched with mature dentate granule neurons (~90% NeuN⁺ neurons)¹⁸.

DNA constructs. The mouse *c-Fos* open reading frame was cloned from adult mouse dentate gyrus 1 h after neuronal activation. AAV gene delivery vectors were constructed by cloning the EF1a-Gene-WPRE and U6-shRNA-EYFP-WPRE cassettes into an AAV backbone²⁰. The following shRNA sequences were used: shRNA-Ctrl: 5'-GTTTCAGATGTGCGGCGAGT-3'; shRNA-cFos: 5'-GCCCTTCCCTACTACCATTC-3'. The efficacy of shRNA against mouse *c-Fos* was confirmed by qPCR using adult mouse dentate gyri after AAV-mediated expression, followed by electroconvulsive stimulation. The following sequence primers for qPCR were used:

Actb (actin)-Forward: 5'-TAGGCACCAGGGTGTGATGG-3'; *Actb*-Reverse: 5'-CATGGCTGGGGTGTGAAGG-3';

c-Fos-Forward: 5'-GGGAATGGTGAAGACCGTGTCA-3'; *c-Fos*-Reverse: 5'-GCAGCCATCTTATCCGTTCCC-3'.

ATAC-seq library construction, sequencing, mapping and data analysis. The transposome assay was performed as previously described¹⁷. Around 50,000 nuclei from each dentate gyrus were used. qPCR was used to estimate of the number of additional cycles needed to generate products at 25% saturation. Typically, four to seven additional PCR cycles were added to the initial set of five cycles. The library was purified on AMPure XP beads (Beckman A63881) and analyzed on an Agilent Bioanalyzer, and 50-bp paired-end sequencing was performed using an Illumina HiSeq 2500 platform according to standard operating procedures. Sequencing reads were mapped to a mouse genome assembly (mm9) from the UCSC genome browser (<http://genome.ucsc.edu/>) using Bowtie2 (ref. 46). Duplicate reads were marked and removed by PICARD Tools (<http://broadinstitute.github.io/picard/>). Open chromatin peaks were analyzed using MACS (ref. 47) software. Differential peaks between different conditions were generated by diffReps (ref. 48). Significant overlap between two sets of genomic regions was tested using GAT (ref. 49). HOMER²⁵ was used to annotate those peaks for motif discovery analysis. IGV (ref. 50) and ngsplot (ref. 51) were used for visualization of raw intensities. Statistical analyses were performed using an in-house R script unless otherwise specified.

RNA-seq and data analyses. Total RNA was purified from adult mouse dentate gyrus of independent samples using an RNeasy kit (Qiagen), DNase I one-column digestion was performed to avoid genomic DNA contamination. Sequencing libraries were prepared using NEBNext Ultra RNA Library Prep kit for Illumina (E7530L) following the manufacturer's protocol. Briefly, total RNA was poly-A tail-selected and then heat-fragmented. The fragmented RNA was reverse-transcribed and the second strand was synthesized to make double stranded DNA. After end repair and 3' adenylation, adapters for multiplexing were ligated to the end of double stranded DNA fragments. The ligation products were amplified and purified to generate Illumina compatible libraries. Sequencing was performed with 100-bp single- or paired-end sequencing by an Illumina HiSeq 2500 or NextSeq 500. The raw reads were mapped to the mouse genome mm9 build

using TopHat (ref. 52). Differential gene expression and downstream analyses were performed using cuffdiff (ref. 53) and custom R scripts.

ChIP-qPCR analysis. Chromatin immunoprecipitation analysis was performed as previously described⁵⁴. Briefly, dentate gyri from mice (E0, E1, E4) were microdissected on ice and subjected to ChIP using an anti-c-Fos antibody (Santa Cruz Biotechnology, sc-7202) following the manufacturer's instructions. The following sequence primers for qPCR were used in PCR to detect the presence of specific DNA binding to c-Fos:

Nrxn3-Forward: 5'-GGCCTTTGTGGAGAATGAGA-3'; *Nrxn3*-Reverse: 5'-TTGTGGCTGGCTCTGTATTG-3';

Gria2-Forward: 5'-GGTTTGTCCCAGGCTGACTA-3'; *Gria2*-Reverse: 5'-GCAGCCTTCCTTTCTCTGAC-3';

Kcnj6-Forward: 5'-ATTCAGCGTCTTTGGGTTTG-3'; *Kcnj6*-Reverse: 5'-GCCTTAGGCTGTGTCAGAGG-3';

Kcnv2-Forward: 5'-TTTGAACCATAGCACCGACA-3'; *Kcnv2*-Reverse: 5'-GACTGCGAGGGTGTTTTCTC-3';

Hivp3-Forward: 5'-CCCCCTCTCTTGAGTCAGTG-3'; *Kcnv2*-Reverse: 5'-GTCTGGCAGAAAAGGCTGTC-3';

Nr3c1-Forward: 5'-CTGCACGGGATCTCATTTTTT-3'; *Nr3c1*-Reverse: 5'-GGAGTAAATGGCAGATGGA-3'.

FAIRE-qPCR analysis. FAIRE was performed following the previously published protocol^{55,56}. Briefly, microdissected dentate gyri were cross-linked with 1% formaldehyde for 5 min and stopped with 0.125 M glycine for 5 min. The washed pellets were resuspended and incubated for 10 min sequentially in 1 ml of buffer L1 (50 mM HEPES-KOH, pH 7.5, 140 mM NaCl, 1 mM EDTA, 10% glycerol, 0.5% NP-40, 0.25% Triton X-100, 1× protease inhibitor) at 4 °C for 10 min, 1 mL buffer L2 (10mM Tris-HCl, pH 8.0, 200 mM NaCl, 1 mM EDTA, 0.5 mM EGTA, 1× protease inhibitor) at room temperature 22 °C for 10 min and 400 µl of buffer L3 for 10 min (10 mM Tris-HCl, pH 8.0, 100 mM NaCl, 1 mM EDTA, 0.5 mM EGTA, 0.1% sodium deoxycholate, 0.5% *N*-lauroylsarcosine, 1× protease inhibitor). The lysates were sonicated in order to shear chromatin into DNA fragments of average 300–500 bp and then centrifuged at 14,000g for 10 min to remove the cellular debris. Input samples were reverse cross-linked overnight at 65 °C. The FAIRE samples and reverse cross-linked input samples were subjected to three sequential phenol/chloroform/isoamyl alcohol (25/24/1) extractions. DNA was precipitated with ethanol, air-dried, dissolved in 100 µL of TE and treated with 1 µl of RNase A (10 mg/ml) for 1 h at 37 °C. Proteins were then digested by proteinase K at 55 °C for 1 h. The DNA was purified with QIAquick PCR Purification Kit (Qiagen) and eluted with 30 µL ddH₂O. The following sequence primers for qPCR were used in PCR to validate the chromatin opening and closing at E0 and E1:

Arc_1-Forward: 5'-TTTCTTAGGGAGCAGCTGGA-3'; *Arc_1*-Reverse: 5'-CTAACCAAAGGCAGCTGAGG-3';

Arc_2-Forward: 5'-CAAGAACCCCTTCTCTC-3'; *Arc_2*-Reverse: 5'-GAAGGGTGTGAGTGGGCTAA-3';

Arc_3-Forward: 5'-CCATAGCTCCTCTGGGAACA-3'; *Arc_3*-Reverse: 5'-CCATAGCTCCTCTGGGAACA-3';

Arc_4-Forward: 5'-GATTTGGTGGCTGTTTCT-3'; *Arc_4*-Reverse: 5'-CCTCCCATGGCTCTTACTCA-3';

Arc_5-Forward: 5'-CGTTTACGAGGAGCAAG-3'; *Arc_5*-Reverse: 5'-CTTGGGCTTCAAACCATTA-3';

Gabrr1-Forward: 5'-CCATAGCTCCTCTGGGAACA-3'; *Gabrr1*-Reverse: 5'-CCATAGCTCCTCTGGGAACA-3'.

Learning combinatorial chromatin states. ChromHMM was used to learn combinatorial chromatin states⁵⁷. ChromHMM was trained using all seven chromatin marks (H3K4me1, H3K4me3, H3K27Ac, H3K27me3, H3K9me3, H4K20me1 and H3K36me3) and CTCF in virtual concatenation mode across all conditions. Reads from replicate data sets were pooled before learning the states. The ChromHMM parameters used are as follows: reads were shifted in the 5' to 3' direction by 100 bp; for each ChIP-seq data set, read counts were computed in non-overlapping 200-bp bins across the entire genome; and each bin was discretized into two levels, 1 indicating enrichment and 0 indicating no enrichment. The binarization was performed by comparing ChIP-seq read counts to the corresponding whole-cell extract-control read-counts within each

bin and using a Poisson P -value threshold of 1×10^{-4} . We trained several models, with the numbers of states ranging from 12 to 25. We decided to use a 15-state model for all further analyses as it captured all the key interactions among the chromatin marks and larger numbers of states did not capture more interactions. To assign biologically meaningful mnemonics to the states, we used the ChromHMM package to compute the overlap and neighborhood enrichments of each state relative to coordinates of known gene annotations. The trained model was then used to compute the posterior probability of each state for each genomic bin in each condition.

Western blot analysis. Cell extracts were obtained from dentate gyri by resuspension in RIPA buffer (150 mM NaCl, 1.0% IGEPAL CA-630, 0.5% sodium deoxycholate, 0.1% SDS, 50 mM Tris, pH 8.0, with 1 mM freshly added PMSF) followed by 30 min incubation on ice. Protein concentration was detected by BCA. Equal amounts of protein from different samples were loaded, separated by SDS-PAGE gel and transferred to nitrocellulose membranes (GE Healthcare Life Science) for immunoblot analysis. Blots were incubated in blocking buffer (5% bovine milk and 0.1% Tween 20 in PBS, pH 7.4) for 1 h at room temperature and then in anti-c-Fos primary antibodies (Santa Cruz Biotechnology, sc-7202; 1:200) overnight at 4 °C, washed in blocking buffer three times for 10 min each and incubated in corresponding secondary antibody (goat anti-rabbit IgG-HRP, Santa Cruz Biotechnology, sc-2004; 1:500) at room temperature for 2 h. Membranes were stripped and reblotted with mouse anti-actin antibodies (Millipore, MAB1501; 1:3,000) as loading controls. Western blot images were analyzed by ImageJ (**Supplementary Fig. 10**). Statistical significance was determined by ANOVA.

Statistics. No statistical methods were used to predetermine sample sizes, but our sample sizes are similar to those generally employed in the field^{18–20,23–28}. No randomization and blinding were employed. A **Supplementary Methods Checklist** is available.

Data availability. The data that support the findings of this study are available from the corresponding author upon reasonable request. Data have been deposited in the GEO database with accession codes [GSE82015](#) and [GSE86367](#).

44. Ge, S. *et al.* GABA regulates synaptic integration of newly generated neurons in the adult brain. *Nature* **439**, 589–593 (2006).
45. Duan, X. *et al.* Disrupted-In-Schizophrenia 1 regulates integration of newly generated neurons in the adult brain. *Cell* **130**, 1146–1158 (2007).
46. Langmead, B. & Salzberg, S.L. Fast gapped-read alignment with Bowtie 2. *Nat. Methods* **9**, 357–359 (2012).
47. Zhang, Y. *et al.* Model-based analysis of ChIP-Seq (MACS). *Genome Biol.* **9**, R137 (2008).
48. Shen, L. *et al.* diffReps: detecting differential chromatin modification sites from ChIP-seq data with biological replicates. *PLoS One* **8**, e65598 (2013).
49. Heger, A., Webber, C., Goodson, M., Ponting, C.P. & Lunter, G. GAT: a simulation framework for testing the association of genomic intervals. *Bioinformatics* **29**, 2046–2048 (2013).
50. Robinson, J.T. *et al.* Integrative genomics viewer. *Nat. Biotechnol.* **29**, 24–26 (2011).
51. Shen, L., Shao, N., Liu, X. & Nestler, E. ngs.plot: Quick mining and visualization of next-generation sequencing data by integrating genomic databases. *BMC Genomics* **15**, 284 (2014).
52. Trapnell, C., Pachter, L. & Salzberg, S.L. TopHat: discovering splice junctions with RNA-Seq. *Bioinformatics* **25**, 1105–1111 (2009).
53. Trapnell, C. *et al.* Transcript assembly and quantification by RNA-Seq reveals unannotated transcripts and isoform switching during cell differentiation. *Nat. Biotechnol.* **28**, 511–515 (2010).
54. Guo, J.U. *et al.* Distribution, recognition and regulation of non-CpG methylation in the adult mammalian brain. *Nat. Neurosci.* **17**, 215–222 (2014).
55. Giresi, P.G. & Lieb, J.D. Isolation of active regulatory elements from eukaryotic chromatin using FAIRE (formaldehyde assisted isolation of regulatory elements). *Methods* **48**, 233–239 (2009).
56. Simon, J.M., Giresi, P.G., Davis, I.J. & Lieb, J.D. Using formaldehyde-assisted isolation of regulatory elements (FAIRE) to isolate active regulatory DNA. *Nat. Protoc.* **7**, 256–267 (2012).
57. Ernst, J. & Kellis, M. ChromHMM: automating chromatin-state discovery and characterization. *Nat. Methods* **9**, 215–216 (2012).